Comparative Study of Analytical and Numerical Techniques in Modeling Electromagnetic Scattering from Single and Double Knife-Edge in 2D Ground Wave Propagation Problems

Ozlem Ozgun [1], and Levent Sevgi [2]

[1] TED University
Department of Electrical and Electronics Engineering, Ankara, Turkey
ozlem.ozgun@tedu.edu.tr

[2] Dogus University
Department of Electronics and Communications Engineering, 34722, Istanbul, Turkey
lsevgi@dogus.edu.tr

Abstract ─ This paper presents a comparative study of some analytical and numerical techniques in the solution of a classical problem of electromagnetic scattering from single and double knife edge above ground. The results of the analytical exact and asymptotic techniques (such as uniform theory of diffraction, parabolic equation diffraction method) are compared with the two-way split-step parabolic equation method (SSPE), through several numerical simulations. Salutary discussions on their capabilities and limitations are presented. Codes used in the simulations are provided in the end.

Index Terms ─ Diffraction, electromagnetic scattering, geometric optics (GO), ground wave propagation, two-way split-step parabolic equation method, uniform theory of diffraction (UTD).

I. INTRODUCTION

Electromagnetic ground wave propagation over the Earth's surface is affected by several scattering phenomena, such as reflection, refraction, and diffraction. Developing a rigorous method for understanding the effects of varying conditions on ground wave propagation is usually a challenging task because of the vast variability of the medium parameters and also the complexity of the surfaces and obstacles that re-direct the propagating energy. Initially, the prediction of the ground wave propagation problem has been achieved by means of some analytical exact or analytical asymptotic techniques [1-17], which require the geometry to be represented as a member of a set of some canonical geometries. The exact techniques express the solution in the form of infinite series or integral and may serve as reference but might be poorly convergent at high frequencies when the dimensions of the objects are much larger than the wavelength. Asymptotic techniques have been widely used for decades to solve problems at high (usually optical) frequencies. These high-frequency asymptotic (HFA) approaches employ simplified models of electromagnetic wave reflection, refraction and diffraction such as geometric optics (GO), physical optics (PO), geometric theory of diffraction (GTD) [8-9], uniform theory of diffraction (UTD) [10-11], physical theory of diffraction (PTD) [12-13]. The GO model describes only the incident, reflected and refracted waves on the illuminated side of the scatterers. The GTD model is complementary to the GO model, in the sense that it overcomes some limitations of GO by including the diffraction mechanism. However, the GTD model exhibits singularities along the incident and reflection shadow boundaries (ISB and RSB). The uniform theory of diffraction (UTD) model achieves smooth wave behavior along these boundaries. This family (GO, GTD, UTD) is also known as ray tracing techniques in the literature. The PO

Submitted On: Nov. 18, 2011
Accepted On: April 20, 2012

and PTD models, on the other hand, are based on induced currents on the surfaces of the scatterers. The PTD model supplements PO by introducing non-uniform ("fringe") edge currents to incorporate the effect of diffraction into the solution. In spite of simplicity, the asymptotic techniques suffer from two major drawbacks: (i) Solutions are available only for certain canonical objects, such as wedge (or knife-edge), cylinder. (ii) (Unless ray-shooting is not used) vertically-varying refractivity profiles in the troposphere cannot be handled.

With the advances in computers, some numerical techniques have been devised to solve the ground wave propagation problem involving complex geometries and inhomogeneous environments. Split-step parabolic equation (SSPE) method [18-22] has been widely used in propagation modeling because of its capability in modeling both horizontally- and vertically-varying atmospheric refraction (especially ducting) effects. It solves an initial-value problem starting from a source (or an antenna), and marching out in range by computing the field along the vertical direction at each range by means of step-by-step Fourier transformations. The classical SSPE method deals only with forward propagating waves, and thus, it is a one-way model that is valid in the paraxial region. Recently, a two-way SSPE algorithm has been introduced [23, 24] to incorporate the backward propagating waves into the one-way SSPE by utilizing an iterative forward-backward scheme for modeling multipath effects. This algorithm has been served for the public's use via a novel, MATLAB® based software tool (PETOOL) [25]. In spite of several advantages, the SSPE method takes the diffraction effects into account within the paraxial approximation, degrading the accuracy of the approach in deep-shadow regions where the diffracted fields dominate.

The organization of this paper is as follows: In Sec. II, analytical exact and asymptotic methods are briefly formulated. In Sec. III, fundamentals of the two-way SSPE are outlined. In Sec. IV, the techniques are compared through several numerical simulations. In the Appendix, the codes used in the simulations are presented.

Except Sec. II C, the time dependence of the form $\exp(-i\omega t)$ is assumed.

II. ANALYTICAL EXACT AND ASYMPTOTIC MODELS

This section discusses various analytical approaches, belonging to the family of ray-based techniques. The problem of interest is the 2D electromagnetic ground wave propagation where single or multiple knife-edges are located on a flat conducting surface and illuminated by a line-source (see Fig. 1). The problem of single or multiple knife-edge (or wedge in general) suspended in a homogeneous medium is one of the classical, canonical problems, and plays a fundamental role in the construction of the high-frequency asymptotic techniques. If the edges are located on a conducting surface, the image theory can be employed to account for the multiple reflections from the ground or edges. The total field is then obtained by the sum of the direct ray, the reflected rays emanating from image sources, and the diffracted rays from the tip of the edges, by also checking the line-of-sight (LOS) conditions between the source and the observation point. The beauty of this model is that it yields physical insight, and contributions of every ray item can be observed separately.

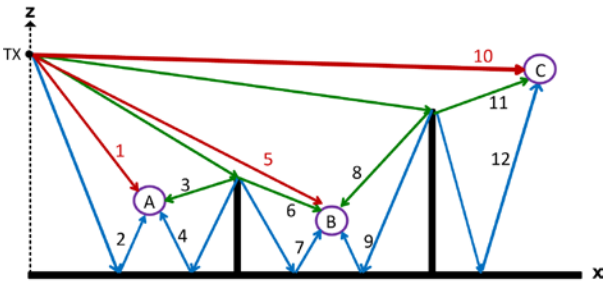

Fig. 1: Geometry of the problem, illustrating some possible ray contributions for different observation points (A, B, C). [Red: direct, Green: diffracted, Blue: reflected or diffracted/reflected].

The subsections below formulate various techniques to modeling of the diffracted field from the tip of a single wedge in the absence of ground (see Fig. 2). The more general problem in Fig. 1 involving multiple bouncing of the rays can be handled by a successive implementation of GO and diffraction algorithms depending on different LOS conditions (this is indeed just a coding issue). The wedge in Fig. 2 is illuminated by a cylindrically diverging line-source. The tip-to-source distance and the source angle are denoted

by r_0 and φ_0, respectively; whereas the tip-to-observer distance and the observation angle are represented by r and φ, respectively. The wedge exterior angle α is set to 2π in the simulations to model the knife-edge. On the other hand, more realistic, hill-type obstacles may be modeled easily by setting $\alpha \neq 2\pi$. The wedge surface is assumed to be perfect electric conductor. As conventional in the diffraction theory, the polarization will be referred to as soft or hard polarizations, which are equivalent to horizontal or vertical polarizations, respectively.

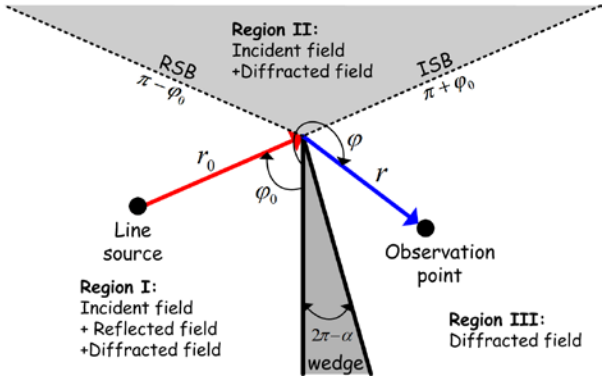

Fig. 2. Problem of scattering from a wedge.

A. Exact series model

Analytical exact solution of the problem in Fig. 2 can be obtained by using the separation of variables method, which reduces the 2D wave equation into two 1D wave equations; one in the angular domain, the other in the radial domain. Depending on the boundary conditions, the angular domain solutions are expressed in terms of sine or cosine functions, whereas the radial domain solutions are constructed by means of Bessel or Hankel functions. Bessel and Hankel functions are appropriate for $r \le r_0$ and for $r > r_0$, respectively.

Assuming a line source of the form of $I_0\delta(r-r_0,\varphi-\varphi_0)$, the exact total field for soft and hard boundary conditions, respectively, are expressed in series as follows: [15]

$$u_s^t = \begin{cases} \dfrac{4\pi}{\alpha}\displaystyle\sum_{m=1}^{\infty} J_{\upsilon_m}(kr)H_{\upsilon_m}^{(1)}(kr_0)\,f_s(\varphi,\varphi_0) & \text{if } r \le r_0 \\ \dfrac{4\pi}{\alpha}\displaystyle\sum_{m=1}^{\infty} J_{\upsilon_m}(kr_0)H_{\upsilon_m}^{(1)}(kr)\,f_s(\varphi,\varphi_0) & \text{if } r \ge r_0 \end{cases} \quad (1)$$

$$u_h^t = \begin{cases} \dfrac{4\pi}{\alpha}\displaystyle\sum_{m=0}^{\infty} \varepsilon_m J_{\upsilon_m}(kr)H_{\upsilon_m}^{(1)}(kr_0)\,f_h(\varphi,\varphi_0) & \text{if } r \le r_0 \\ \dfrac{4\pi}{\alpha}\displaystyle\sum_{m=0}^{\infty} \varepsilon_m J_{\upsilon_m}(kr_0)H_{\upsilon_m}^{(1)}(kr)\,f_h(\varphi,\varphi_0) & \text{if } r \ge r_0 \end{cases} \quad (2)$$

Here, k is the wavenumber, $\upsilon_m = m\pi/\alpha$, $\varepsilon_m = 1/2$ if $m=0$ and $\varepsilon_m = 1$ otherwise; and $f_s = \sin(\nu_m\varphi_0)\sin(\nu_m\varphi)$, $f_h = \cos(\nu_m\varphi_0)\cos(\nu_m\varphi)$.

Since the total field is the sum of the diffracted field and the GO field (i.e., $u_{s,h}^t = u_{s,h}^d + u_{s,h}^{GO}$), the diffracted field $u_{s,h}^d$ can be obtained by subtracting the GO field from the total field. The GO field is the sum of the incident (direct) field and the reflected field emanating from the image source (i.e., $u_{s,h}^{GO} = u_{s,h}^{inc} + u_{s,h}^{r}$ where $u_{s,h}^{r} = u_{s,h}^{inc,image}$). The incident field is expressed in terms of Hankel function, i.e., $u_s^{inc} = H_0^{(1)}(kR)$, where R is the distance between the source (actual or image) and observation points (i.e., R_{actual} or R_{image}). Hence, the GO field can be expressed with respect to the LOS conditions, as follows:

$$u_{s,h}^{GO} = \varepsilon_1 H_0^{(1)}(kR_{actual}) \mp \varepsilon_2 H_0^{(1)}(kR_{image}), \quad (3)$$

where (-) and (+) are for soft and hard polarizations, respectively. Moreover,

$$\varepsilon_1 = \begin{cases} 1 \text{ for } \varphi \le \pi+\varphi_0 \\ 0 \text{ for } \varphi > \pi+\varphi_0 \end{cases}, \quad (4)$$

$$\varepsilon_2 = \begin{cases} 1 \text{ for } \varphi \le \pi-\varphi_0 \\ 0 \text{ for } \varphi > \pi-\varphi_0 \end{cases} \text{ (if } 0 \le \varphi_0 \le \alpha-\pi\text{)}, \quad (5)$$

$$\varepsilon_2 = \begin{cases} 1, \text{ for } 0 < \varphi < \pi-\varphi_0 \\ 0, \text{ for } \pi-\varphi_0 < \varphi < 2\alpha-\pi-\varphi_0 \\ 1, \text{ for } 2\alpha-\pi-\varphi_0 < \varphi < \alpha \end{cases} \text{ (if } \alpha-\pi \le \varphi_0 \le \pi\text{)} \quad (6)$$

Note that the case $0 \le \varphi_0 \le \alpha-\pi$ in (5) and $\alpha-\pi \le \varphi_0 \le \pi$ in (6) refer to Single-Side (only one face) and Double-Side illuminations, respectively.

Under the conditions where $kr_0 >> 1$ and $kr >> 1$, asymptotic forms of Hankel functions can be used. Hence, the diffracted field can be cast into the following form:

$$u_{s,h}^d = u_0 d_{s,h} \frac{e^{ikr}}{\sqrt{r}}, \quad (7)$$

where $u_0 = H_0^{(1)}(kr_0)$ is the incident field at the tip of the wedge, and $d_{s,h}$ is the *diffraction coefficient*.

Thus, (7) allows us to compute the diffraction coefficient approximately after the exact diffracted field is computed, i.e., $d_{s,h} = \sqrt{r}\left(u_{s,h}^{d}/u_0\right)\mathrm{e}^{-ikr}$.

It is useful to note that the number of terms in the series expressions increases drastically as the frequency increases and/or the observation point moves away from the tip of the wedge. This might obviously place a bottleneck on the computation time during the numerical implementation.

B. Exact integral model

Analytical exact solution of the wedge diffraction problem can also be obtained by an integral representation presented by Bowman & Senior in a handbook [6]. The diffracted fields can be expressed as allows:

$$u_{s,h}^{d} = \left[V_d(-\pi-\varphi+\varphi_0) - V_d(\pi-\varphi+\varphi_0)\right] \mp \left[V_d(-\pi-\varphi-\varphi_0) - V_d(\pi-\varphi-\varphi_0)\right], \quad (8)$$

where (-) and (+) are for soft and hard polarizations, respectively. Here,

$$V_d(\beta) = \frac{1}{2\pi n}\int_0^{\infty} H_0^{(1)}[kR(i\kappa)]\frac{\sin(\beta/n)}{\cosh(\kappa/n)-\cos(\beta/n)}d\kappa \quad (9)$$

where $n = \alpha/\pi$ and $R(\eta) = \sqrt{r^2 + r_0^2 + 2rr_0\cos(\eta)}$.

Note that the total fields can be determined by adding the GO fields to the diffracted fields in (8). Similarly, the diffracted field can be expressed in the form of (7), from which the diffraction coefficient is calculated. Away from the shadow boundaries, asymptotic form of the diffraction coefficient can be derived as follows:

$$d_{s,h}^{asymp} = \frac{\sin(\pi/n)}{n}\left[\left(\cos\frac{\pi}{n} - \cos\frac{\varphi-\varphi_0}{n}\right)^{-1} \mp \left(\cos\frac{\pi}{n} - \cos\frac{\varphi+\varphi_0}{n}\right)^{-1}\right]\frac{\mathrm{e}^{i\pi/4}}{\sqrt{2\pi k}}, \quad (10)$$

where (-) and (+) are for soft and hard polarizations, respectively. Here, the complex exponential term $\mathrm{e}^{i\pi/4}$ indicates that the wedge tip is the caustic of edge-diffracted rays. Note that the critical part of this representation is the numerical integration of the $V_d(\beta)$ integral in (9), which contains singularities on the complex β plane because of Hankel function and the denominator [26]. Since the direct numerical integration along positive real axis is very time consuming, a deformed contour can be used to accelerate the computations.

C. Uniform theory of diffraction (UTD) model

In this model, the diffracted field is also expressed in the same form in (7), except that $u_0 = H_0^{(2)}(kr_0)$ and $\mathrm{e}^{i\pi/4}$ is replaced by $\mathrm{e}^{-j\pi/4}$ due to the time dependence convention in UTD. The UTD diffraction coefficients are given as [10]:

$$d_{s,h} = \frac{-e^{-j\pi/4}}{2n\sqrt{2\pi k}}\left\{\left[\cot\left(\frac{\pi-\xi^-}{2n}\right)F(kLg^+\xi^-) + \cot\left(\frac{\pi+\xi^-}{2n}\right)F(kLg^-\xi^-)\right] \mp \left[\cot\left(\frac{\pi-\xi^+}{2n}\right)F(kLg^+\xi^+) + \cot\left(\frac{\pi+\xi^+}{2n}\right)F(kLg^-\xi^+)\right]\right\}, \quad (11)$$

where (-) and (+) are for soft and hard polarizations, respectively. Furthermore, $\xi^+ = \varphi+\varphi_0$, $\xi^- = \varphi-\varphi_0$ and $F(X)$ is the Fresnel function given as follows:

$$F(X) = 2j\sqrt{X}e^{jX}\int_{\sqrt{X}}^{\infty} e^{-j\tau^2}d\tau, \quad (12)$$

and L, $g^{\pm}$ are computed as follows:

$$L = \frac{rr_0}{r+r_0},\ g^{\pm}(\xi) = 2\cos^2\left(\frac{2n\pi N^{\pm}-\xi}{2}\right), \quad (13)$$

where $N^{\pm} = (\pm\pi+\xi)/2n\pi$ are the integers that most closely satisfy this expression.

Note that the cotangent functions in (11) possess singularities at the shadow boundaries, and hence, can be replaced by the following:

$$\cot\left(\frac{\pi\pm\beta}{2n}\right)F\left(kLg^{\pm}\xi\right) \simeq n\left[\sqrt{2\pi kL}\,\mathrm{sgn}(\varepsilon) - 2kL\varepsilon e^{-j\pi/4}\right]e^{-j\pi/4}, \quad (14)$$

for small $\varepsilon \to 0$. Similarly, the total fields are obtained by adding the GO and the diffracted fields, according to the LOS conditions. Finally, note that the UTD diffraction coefficients are equivalent to (10) away from the shadow boundaries, by replacing $\mathrm{e}^{i\pi/4}$ with $\mathrm{e}^{-j\pi/4}$.

C. Parabolic equation (PE) model

The parabolic equation (PE) diffraction method provides a correct first-order approximation to the diffracted field in the case when $kr >> 1$ and $kr_0 >> 1$ [13]. Note that, in spite of the similarity of

name, this model is different from the split-step parabolic equation (SSPE) method, which is a numerical marching type algorithm described in Sec. III. The PE-based diffracted field can be determined as follows:

$$u_{s,h}^{d} = u_0 \sqrt{\frac{r_0}{r_0 + r}} W_{s,h}(k\rho, \varphi, \varphi_0)\, \mathrm{e}^{ikr}, \quad \rho = \frac{r r_0}{r + r_0}, \tag{15}$$

where

$$W_{s,h}(k\rho, \varphi, \varphi_0) = w(k\rho, \varphi - \varphi_0) \mp w(k\rho, \varphi + \varphi_0), \tag{16}$$

where (-) and (+) are for soft and hard polarizations, respectively. Here,

$$w(k\rho,\psi)\,\mathrm{e}^{ik\rho} = \frac{1}{\pi\sqrt{2}}\,\mathrm{e}^{i(k\rho+\pi/4)} \int_{-\infty}^{\infty} \mathrm{e}^{-k\rho s^2} \frac{\frac{1}{n}\sin\frac{\pi}{n}}{\cos\frac{\pi}{n} - \cos\frac{\eta(s)+\psi}{n}} ds, \tag{17}$$

which is equivalent to the following form:

$$\begin{aligned} w(k\rho,\psi)\,\mathrm{e}^{ik\rho} = {} & \frac{1}{\pi\sqrt{2}} e^{i(k\rho+\frac{\pi}{4})} \int_{-\infty}^{\infty} e^{-k\rho s^2} \Big[\frac{1}{2n}\cot\frac{\eta(s)+\psi-\pi}{2n} \\ & -\frac{1}{2}\csc\frac{\varsigma(s)+\psi-\pi}{2}\sec\frac{\zeta(s)}{2} \\ & -\frac{1}{2n}\cot\frac{\eta(s)+\psi+\pi}{2n}\Big] ds \\ & + e^{-ik\rho\cos\psi}\frac{e^{-i\pi/4}}{\sqrt{\pi}} \int_{\sqrt{2k\rho}\sin\frac{\psi-\pi}{2}}^{\sin\frac{\psi-\pi}{2}} e^{ix^2} dx \end{aligned} \tag{18}$$

where $\eta = \sqrt{2} s\, \mathrm{e}^{-i\pi/4}$, $s = \sqrt{2}\,\mathrm{e}^{-i\pi/4}\sin\zeta/2$ and $\zeta(s) = -i\ln(1 + is^2 + is\sqrt{s^2 - 2i})$. This form is convenient for numeric calculation and asymptotic evaluation [26]. In the vicinity of the saddle point ($|s| << 1$), the following approximations can be made:

$$\zeta(s) = s\sqrt{2}\,\mathrm{e}^{-i\pi/4} + O(s^2) = \eta(s) + O(s^2), \tag{19a}$$

$$\sec\frac{\zeta(s)}{2} = 1 + O(s^2). \tag{19b}$$

Thus, the two first terms in the square brackets of (18), which are singular at the saddle point when $\psi = \varphi \pm \varphi_0 = \pi$, completely cancel each other and the standard saddle point technique can be applied to the integral over the variable s.

Finally, the diffraction coefficients are found as follows:

$$d_{s,h} = W(k\rho, \varphi, \varphi_0)\sqrt{\frac{r r_0}{r + r_0}}, \tag{20}$$

which reduces to (10) away from the shadow boundaries.

III. TWO-WAY SPLIT-STEP PARABOLIC EQUATION MODEL

The parabolic wave equation (PWE) is derived from the 2D Helmholtz wave equation by separating the rapidly varying phase term to obtain a reduced function varying slowly in range for propagating angles close to the paraxial (horizontal) direction. The PWE can be converted to an initial value problem and can be solved by a marching-type numerical algorithm. The Fourier split-step parabolic equation (SSPE) is a powerful algorithm which accepts the initial field at a reference range (e.g., at an antenna) and then advances in range by computing the field along longitudinal direction at each range step. The classical SSPE is known as one-way approach because it handles only the forward-propagating waves, and cannot account for the backscattered ones. The classical one-way SSPE determines the longitudinal field at range $x + \Delta x$ as follows [20]:

$$\begin{aligned} u(x + \Delta x, z) = {} & \exp\left[ik(n^2 - 1)\frac{\Delta x}{2} \right] \times \\ & F^{-1}\left\{ \exp\left[-ip^2 \frac{\Delta x}{2k} \right] F\{u(x,z)\} \right\} \end{aligned} \tag{21}$$

where F denotes the Fourier Transform, $p = k_z$ is the transform variable (i.e., transverse wavenumber $p = k\sin\theta$ where θ is the propagation angle from the horizontal), and n is the refractive index. Eqn. (21) is valid for propagation angles up to 10°-15°, and hence, it is known as narrow-angle SSPE. Long-range propagation can be accurately modeled with the narrow-angle SSPE because propagation angles encountered in such problems are usually less than a few degrees. However, short range propagation problems, as well as the problems involving multiple reflections and diffractions because of hills and valleys with steep slopes, can be modeled more accurately with the wide-angle SSPE, which is effective for propagation angles up to 40°-45° [22, 25]. The wide-angle SSPE obtains the field at each range as follows:

$$\begin{aligned} u(x + \Delta x, z) = {} & \exp\left[ik(n-1)\Delta x \right] \times \\ & F^{-1}\left\{ \exp\left[ik\Delta x\left(\sqrt{1 - \frac{p^2}{k^2}} - 1 \right) \right] F\{u(x,z)\} \right\} \end{aligned} \tag{22}$$

Although the one-way SSPE model is quite effective in modeling electromagnetic propagation above the Earth's irregular surface through inhomogeneous atmosphere, it suffers from the disability of handling backward-propagating waves. The forward waves might be sufficient for long-range propagation scenarios. However, the backward waves become significant in the presence of obstacles that re-direct the incoming wave, which renders a necessity of estimating the multipath effects accurately. Recently, a two-way SSPE algorithm was implemented in [23] to incorporate the backward-propagating waves into the solution, through a recursive forward-backward scheme to model the electromagnetic propagation over a staircase-approximated terrain (i.e., the terrain is modeled like a train of knife-edges). If the wave meets the terrain (or knife-edge), it is partially-reflected by imposing the appropriate boundary conditions on the terrain facet, and is marched out in the backward direction by reversing the paraxial direction in the PWE formulation. Note that the same form of (22) is used during the backward propagation. At each step where the wave hits the terrain, the wave is split into two components (forward and backward). Each wave component continues to march out in its own paraxial direction. The convergence of the algorithm is checked against a certain threshold criterion comparing the total fields at each iteration. The two-way SSPE algorithm was implemented in MATLAB and presented as a software tool (called PETOOL), which can be downloaded from [25].

IV. NUMERICAL SIMULATIONS

This section demonstrates the test results of the analytical and numerical techniques over different propagation scenarios. The first scenario involves a single knife-edge of height 150 m located at 3 km. The line-source is at 50 m height; the frequency is 300 MHz; and the polarization is soft. The 3D maps of the propagation factor[1] within the entire domain are plotted in Fig. 3. Note that the exact models are not included in this figure because they are extremely time-consuming.

A good agreement is observed among the results of the analytical techniques. When the two-way SSPE is compared with the analytical techniques, a good conformity is obtained in the region before 3 km that is in the interference region, but a slight discrepancy is observed in the region after 3 km that is in the deep-shadow / diffraction region. This discrepancy might be due to ignoring some of the less contributing ray components, and/or due to the limitation of SSPE within the paraxial regions. It is also observed that artificial effects around the shadow boundaries are clearly apparent on the maps of the analytical methods. However, SSPE model provides smoother wave behavior around the transition regions.

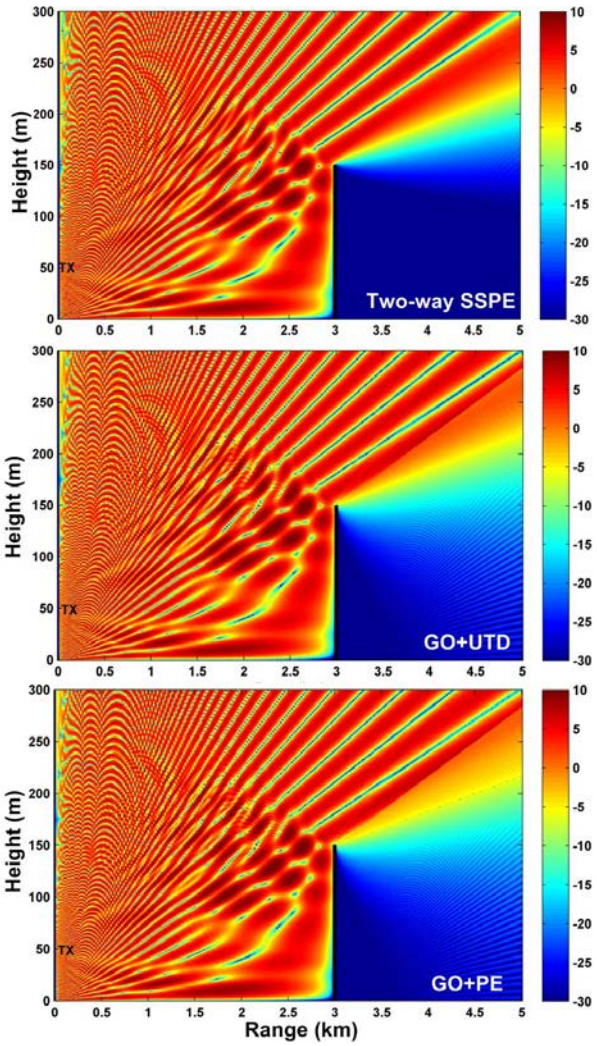

Fig. 3. 3D PF maps for a single knife edge above ground at 3 km range illuminated by a line-source at 50 m height (soft polarization): (a) Two-way SSPE, (b) GO+UTD, (c) GO+PE [f = 300 MHz].

[1] The propagation factor (PF) is the field strength relative to its free-space value in dB.

All techniques are also compared in Fig. 4, which shows the polar plot of the total field along a circle of radius 50 m centered at the tip of the single knife edge. In addition, in Figs. 5(a) and 5(b), the PF values are plotted at two different values of range (2.8 km and 4 km, which are in interference and shadow regions, respectively). In Figs. 5(c) and (d), similarly, the values are plotted at different height values (140 m and 160 m). It is concluded from the results that all analytical methods are in good harmony with each other. The results of the two-way SSPE are slightly different in the shadow region, as discussed above. However, it is remarkable to emphasize that the efficiency of the two-way SSPE, in terms of the computation time, is quite superior to the analytical techniques. Moreover, the two-way SSPE can easily be applied to any type of terrain or any number of knife-edges with little effort. If the analytical techniques are sorted according to the computation time, UTD is the fastest, and then the PE, exact integral and exact series methods come in order. But, especially in the exact methods, the computation time is highly dependent on the frequency and the distance between the observation point and the edge. Note that analytical exact models serve as reference if numerically computed accurately.

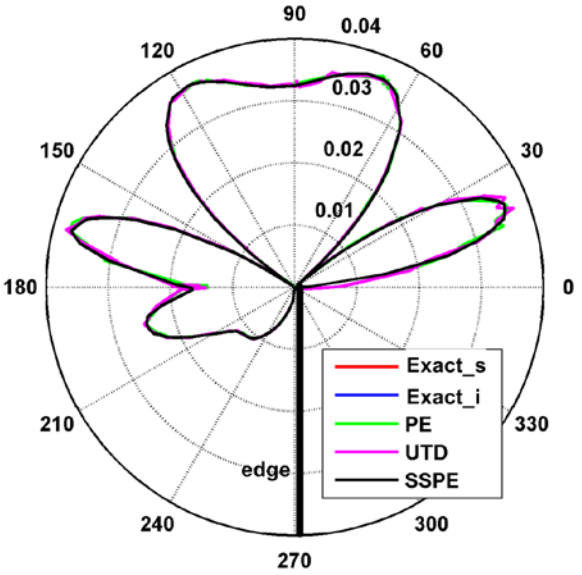

Fig. 4. Polar plot of the total field along a circle of radius 50 m centered at the tip of the single knife edge shown in Fig. 3. [s: series, i: integral].

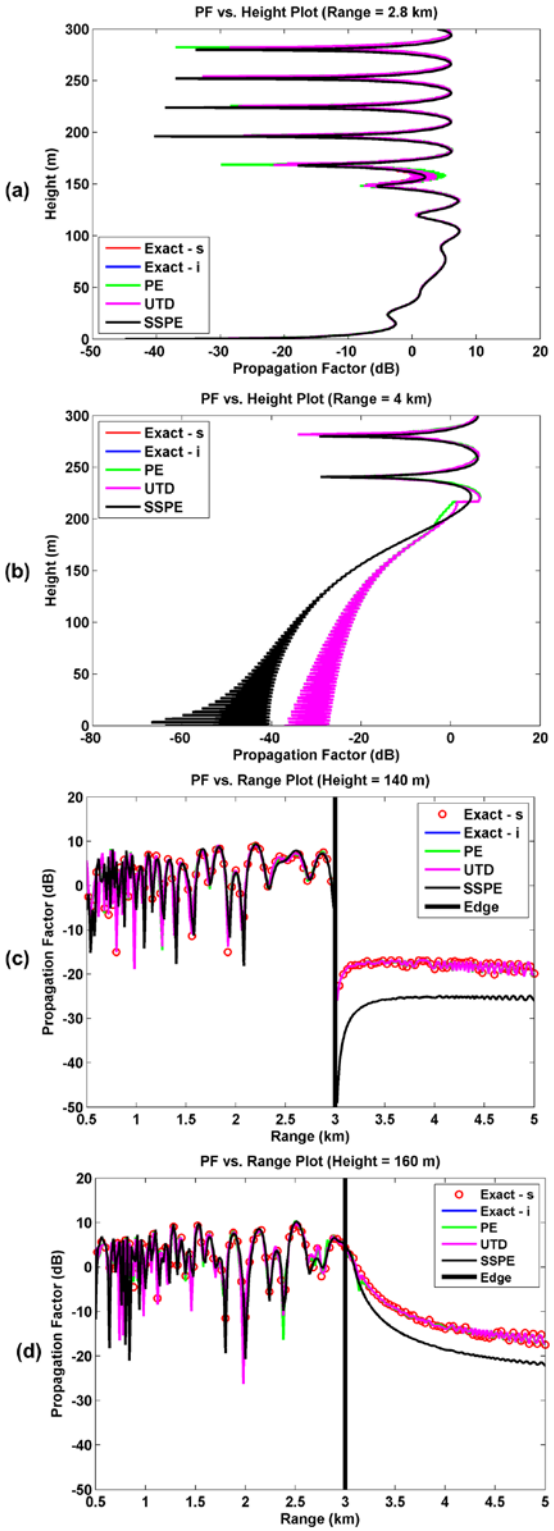

Fig. 5. 2D PF plots for the single knife edge problem shown in Fig. 3: (a) PF vs. height at 2.8 km range, (b) PF vs. height at 4 km range, (c) PF vs. range at 140 m height, (d) PF vs. range at 160 m height. [s: series, i: integral].

The second scenario is the same as the first one, except that the polarization is hard and the line-source is at 100 m height. The results are plotted in Figs. 6, 7, and 8. Again, a good agreement is observed among different models.

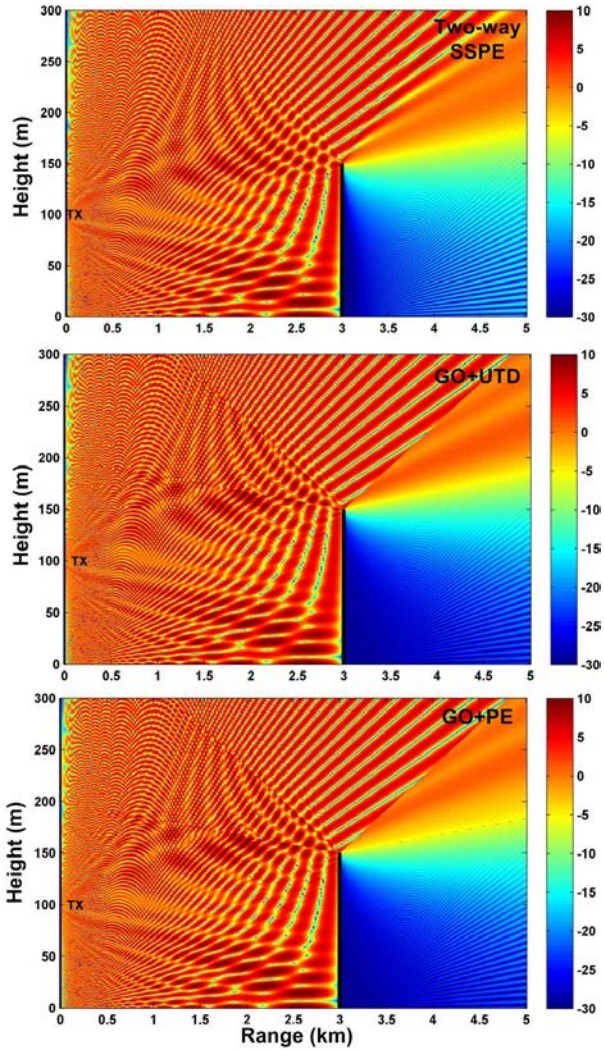

Fig. 6. 3D propagation factor maps for a single knife edge above ground at 3 km range illuminated by a line-source at 100 m height (hard polarization): (a) Two-way SSPE, (b) GO+UTD, (c) GO+PE. [f = 300 MHz].

The last scenario considers double knife-edge of heights 150 m and 170 m located at 3 km and 5 km, respectively. The line-source is at 25 m height; the frequency is 300 MHz; and the polarization is soft. The results are plotted in Figs. 9, 10, and 11. In comparing the two-way SSPE with the analytical methods, the contributions of the waves hitting the walls up to 3 times are superposed. To achieve fair comparisons up to the third degree of reflections, the analytical methods account for 35 types of rays bouncing from the walls and the ground. The multiple bouncing of the diffracted fields from the walls and the ground is ignored due their negligible effects compared to strong reflections.

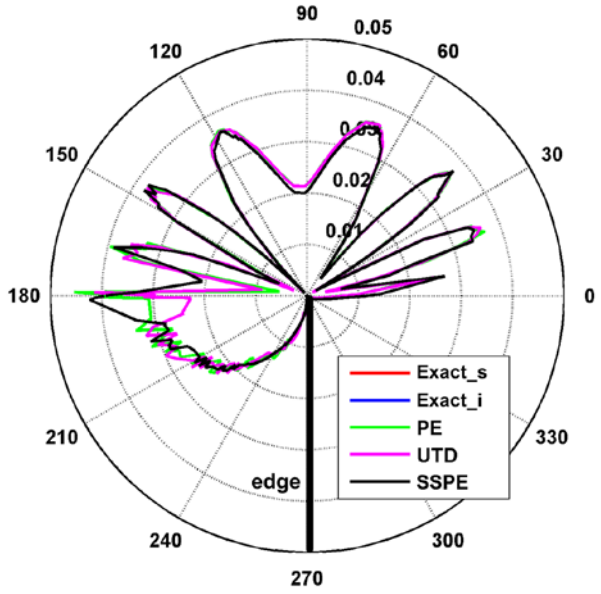

Fig. 7. Polar plot of the total field along a circle of radius 50 m centered at the tip of the single knife edge shown in Fig. 6. [s: series, i: integral].

Again, a good agreement is observed especially in the regions where strong multipath effects are observed, but some discrepancies exist between SSPE and the diffraction algorithms in the deep shadow region.

Simulations with double knife-edges and with other frequencies are repeated for the other polarization (i.e., hard boundary condition) and similar agreement among the models are obtained.

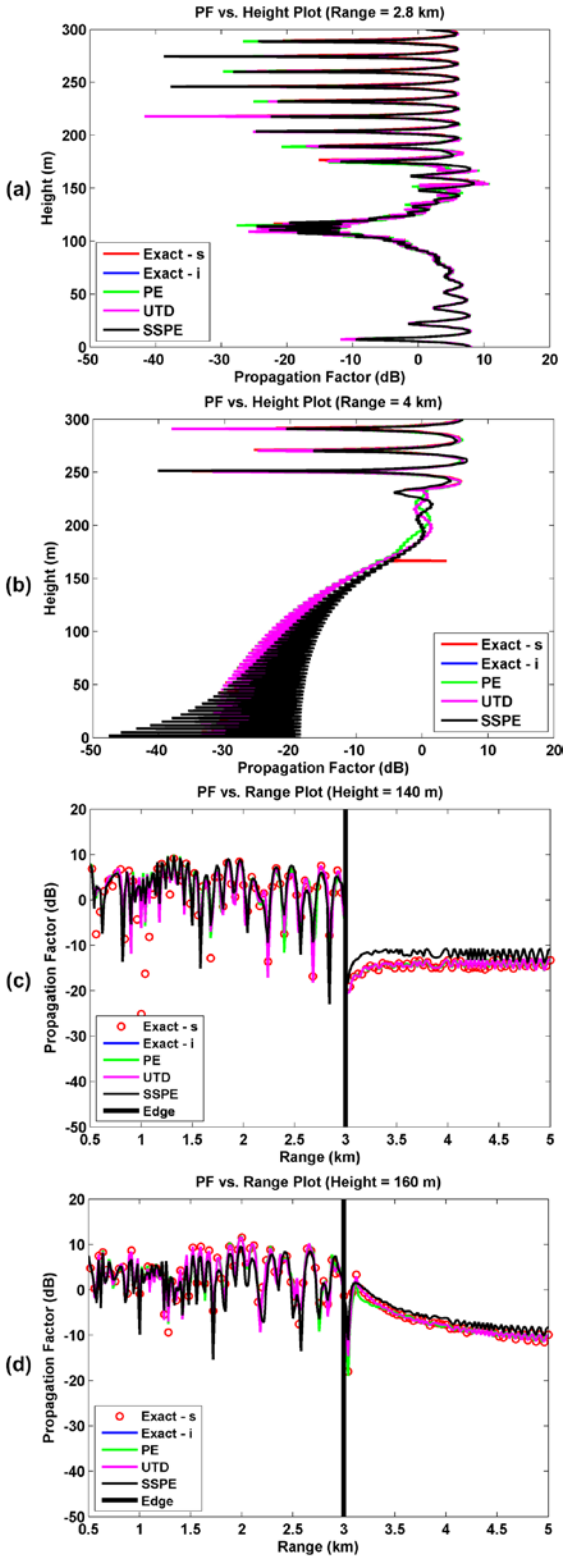

Fig. 8. 2D PF plots for the single knife edge problem shown in Fig. 6: (a) PF vs. height at 2.8 km range, (b) PF vs. height at 4 km range, (c) PF vs. range at 140 m height, (d) PF vs. range at 160 m height. [s: series, i: integral].

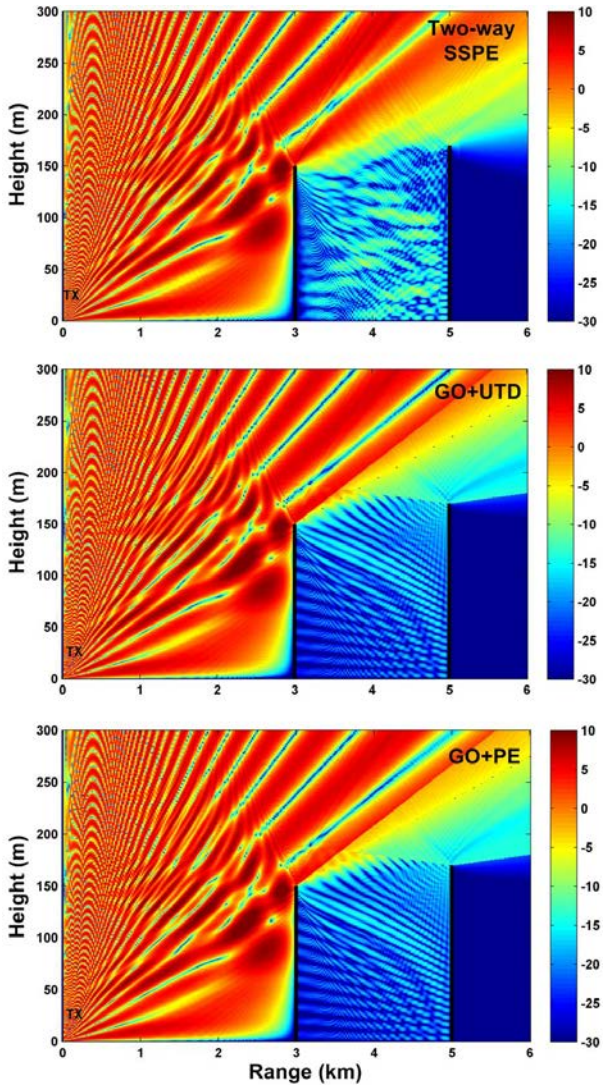

Fig. 9. 3D propagation factor maps for double knife edge above ground at 3 km and 5 km ranges illuminated by a line-source at 25 m height (soft polarization): (a) Two-way SSPE, (b) GO+UTD, (c) GO+PE. [f = 300 MHz].

V. CONCLUSION

Analytical (exact and asymptotic) techniques and the two-way SSPE were discussed and compared through several numerical simulations in the context of the problem of scattering from single and double edge above ground. It was concluded that the results are in good agreement in general, however, some differences might be observed in the deep shadow region or around the shadow boundaries. The disparity of the two-way SSPE in the shadow region, which indeed exhibits "small" field values, might be tolerated in favor of

its computational efficiency. Finally, MATLAB-based codes were provided in Appendix.

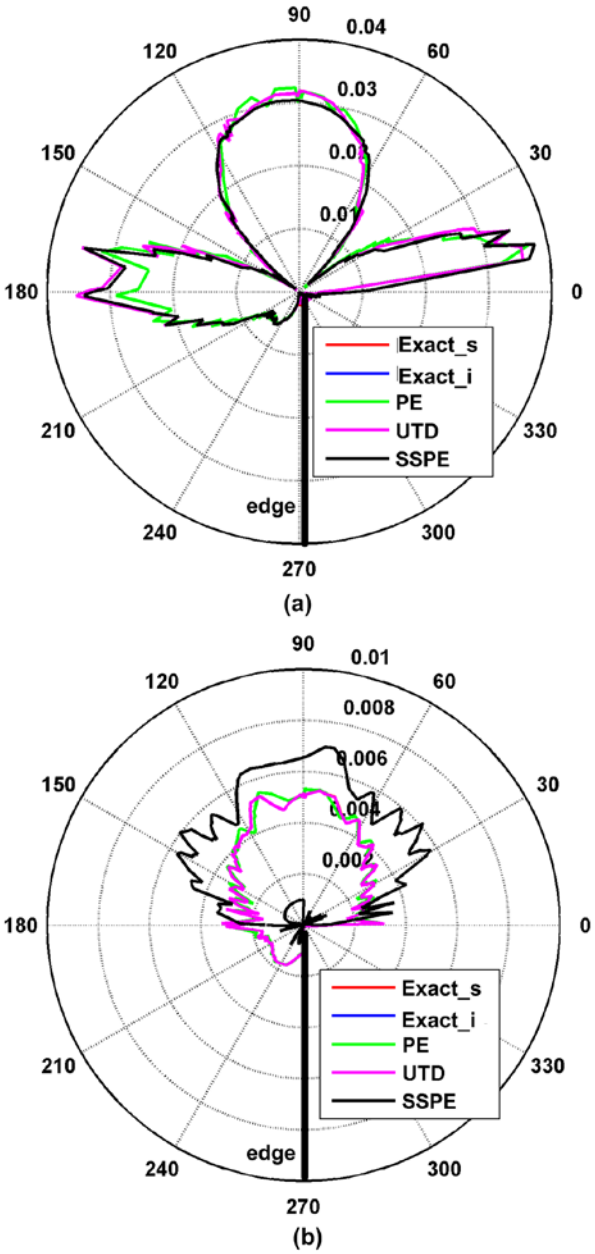

Fig. 10. Polar plot of the total field along a circle of radius 50 m centered at the tip of each knife edge shown in Fig. 9: (a) Edge at 3 km range, (b) Edge at 5 km range. [s: series, i: integral].

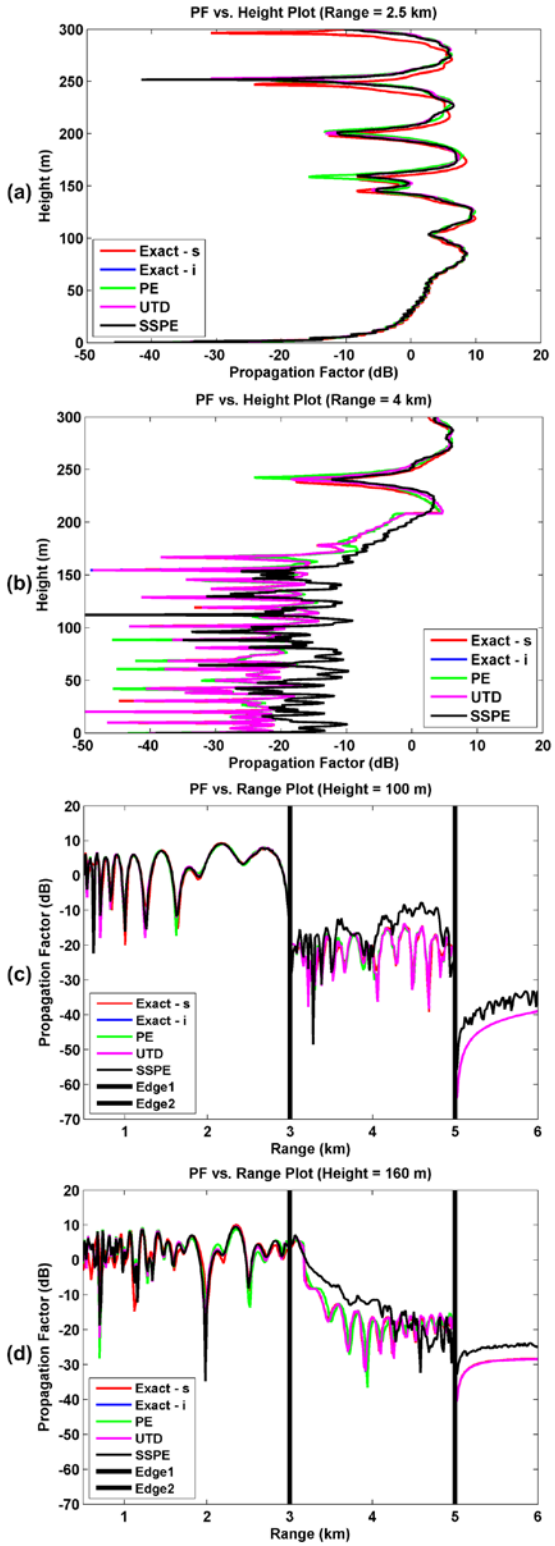

Fig. 11. 2D propagation factor (PF) plots for the double knife edge problem shown in Fig. 9: (a) PF vs. height at 2.5 km range, (b) PF vs. height at 4 km range, (c) PF vs. range at 100 m height, (d) PF vs. range at 160 m height. [s: series, i: integral].

APPENDIX
MATLAB Codes

Sample codes for the diffraction algorithms in Sec. II are given in Tables 1-5 below. The codes computing the 3D field maps of the single or double edge problem (with respect to various LOS conditions) can be provided upon request from the authors. Note that the two-way SSPE algorithm (PETOOL) can be downloaded from [25].

Table 1: Input parameters common to the codes

```
clear all; format long;
freq = 300; %input('frequency [MHz] = ');
alfamax = 360; %input('wedge angle [Deg] = ');
I0 = 1; %input('strength of line source  = ');
r = 50; %input('distance of the observer to wedge  = ');
r0 = 212; %input('distance of the source to wedge  = ');
ang0 = 45; %input('incident angle [Deg] = ');
ang = 150; %input('observation angle [Deg] = ');
c = 3e8; % speed of light
alfa = alfamax*pi/180; % change wedge angle degree to radians
ang0 = ang0*pi/180; % change incident angle degree to radians
ang = ang*pi/180;  % change observation angle degree to radians
error = 1e-12;
freq = freq*1e6; rlam = r*freq/c; k = 2*pi*freq/c;  kr = k*r; kr0 = k*r0;
```

Table 2: Code of the exact by series method

```
Us=0; Uh=0; n=0; vn=0;   err1 = 1e6; err2 = 1e6;  coeff1 = pi*I0/(1i*alfa);
U0 = I0*besselh(0,1,kr0)/(4*1i);
% define N for Soft BSc
 while (err1 > error)
    vn1 = n*pi/alfa;  vn2 = (n+1)*pi/alfa;   vn3 = (n+2)*pi/alfa;
    vn4 = (n+3)*pi/alfa;  vn5 = (n+4)*pi/alfa;
    if r <= r0
      a1 = besselj(vn1,kr)*besselh(vn1,1,kr0)*sin(vn1*ang0)*sin(vn1*ang);
      a2 = besselj(vn2,kr)*besselh(vn2,1,kr0)*sin(vn2*ang0)*sin(vn2*ang);
      a3 = besselj(vn3,kr)*besselh(vn3,1,kr0)*sin(vn3*ang0)*sin(vn3*ang);
      a4 = besselj(vn4,kr)*besselh(vn4,1,kr0)*sin(vn4*ang0)*sin(vn4*ang);
      a5 = besselj(vn5,kr)*besselh(vn5,1,kr0)*sin(vn5*ang0)*sin(vn5*ang);
      Xs = a1+a2+a3+a4+a5;  err1 = abs(Xs);
    else
      a1 = besselj(vn1,kr0)*besselh(vn1,1,kr)*sin(vn1*ang0)*sin(vn1*ang);
      a2 = besselj(vn2,kr0)*besselh(vn2,1,kr)*sin(vn2*ang0)*sin(vn2*ang);
      a3 = besselj(vn3,kr0)*besselh(vn3,1,kr)*sin(vn3*ang0)*sin(vn3*ang);
      a4 = besselj(vn4,kr0)*besselh(vn4,1,kr)*sin(vn4*ang0)*sin(vn4*ang);
      a5 = besselj(vn5,kr0)*besselh(vn5,1,kr)*sin(vn5*ang0)*sin(vn5*ang);
      Xs = a1+a2+a3+a4+a5;  err1 = abs(Xs);
    end
    n=n+1;
 end
N1 = n+10;
% define N for Hard BSc
n=0; vn=0;
while (err2 > error)
    vn1 = n*pi/alfa;  vn2 = (n+1)*pi/alfa;   vn3 = (n+2)*pi/alfa;
    vn4 = (n+3)*pi/alfa;  vn5 = (n+4)*pi/alfa;
    if (n == 0) eps = 0.5; else eps = 1; end
    if r <= r0
   b1 = eps*besselj(vn1,kr)*besselh(vn1,1,kr0)*cos(vn1*ang0)*cos(vn1*ang);
   b2 = eps*besselj(vn2,kr)*besselh(vn2,1,kr0)*cos(vn2*ang0)*cos(vn2*ang);
   b3 = eps*besselj(vn3,kr)*besselh(vn3,1,kr0)*cos(vn3*ang0)*cos(vn3*ang);
   b4 = eps*besselj(vn4,kr)*besselh(vn4,1,kr0)*cos(vn4*ang0)*cos(vn4*ang);
   b5 = eps*besselj(vn5,kr)*besselh(vn5,1,kr0)*cos(vn5*ang0)*cos(vn5*ang);
   Xh = b1+b2+b3+b4+b5; err2 = abs(Xh);
    else
   b1 = eps*besselj(vn1,kr0)*besselh(vn1,1,kr)*cos(vn1*ang0)*cos(vn1*ang);
   b2 = eps*besselj(vn2,kr0)*besselh(vn2,1,kr)*cos(vn2*ang0)*cos(vn2*ang);
   b3 = eps*besselj(vn3,kr0)*besselh(vn3,1,kr)*cos(vn3*ang0)*cos(vn3*ang);
   b4 = eps*besselj(vn4,kr0)*besselh(vn4,1,kr)*cos(vn4*ang0)*cos(vn4*ang);
   b5 = eps*besselj(vn5,kr0)*besselh(vn5,1,kr)*cos(vn5*ang0)*cos(vn5*ang);
   Xh = b1+b2+b3+b4+b5;  err2 = abs(Xh);
    end
    n=n+1;
end
N2 = n+10;  n = 0;
%  Calculating Diffractted  and Total Field
while N1 > n
 vn = n*pi/alfa;
 if n == 0 eps = 0.5; else eps = 1; end
if r <= r0,Us=Us+besselj(vn,kr)*besselh(vn,1,kr0)*sin(vn*ang0)*sin(vn*ang);
else, Us=Us+eps*besselj(vn,kr0)*besselh(vn,1,kr)*sin(vn*ang0)*sin(vn*ang);
end
 n=n+1;
end
n = 0;
while N2 > n
vn = n*pi/alfa;
if n == 0 eps = 0.5; else eps = 1; end
if r <= r0
Uh=Uh+eps*besselj(vn,kr)*besselh(vn,1,kr0)*cos(vn*ang0)*cos(vn*ang);
else
Uh=Uh+eps*besselj(vn,kr0)*besselh(vn,1,kr)*cos(vn*ang0)*cos(vn*ang);
end
n=n+1;
end
Us=Us*coeff1;  Uh=Uh*coeff1;
if (ang >= 0) && (ang < pi-ang0)   % -------- Region I -------
   R1=sqrt(r*r+r0*r0-2*r*r0*cos(ang-ang0));
   R2=sqrt(r*r+r0*r0-2*r*r0*cos(ang+ang0));
   Uxs=I0*besselh(0,1,k*R1)/(4*1i)-I0*besselh(0,1,k*R2)/(4*1i);
   Uxh=I0*besselh(0,1,k*R1)/(4*1i)+I0*besselh(0,1,k*R2)/(4*1i);
   Usdiff = Us-Uxs;    Uhdiff = Uh-Uxh;
elseif  (ang >= pi-ang0) && (ang < pi+ang0)   % -------- Region II -------
   R1=sqrt(r*r+r0*r0-2*r*r0*cos(ang-ang0));
   Ux=I0*besselh(0,1,k*R1)/(4*1i); Usdiff = Us-Ux;    Uhdiff = Uh-Ux;
elseif (ang >= pi+ang0) && (ang <= alfa)  % -------- Region III -------
   Usdiff = Us;    Uhdiff = Uh;
end
UhnTOTAL_SERIES= (Uh/U0);    % exact normalised Total fields hard
UhnDIFF_SERIES=(Uhdiff/U0)*sqrt(2*pi*kr)/exp(1i*kr); % exactdiffco hard
UsnTOTAL_SERIES= (Us/U0);    % exact normalised Total fields Soft
UsnDIFF_SERIES=(Usdiff/U0)*sqrt(2*pi*kr)/exp(1i*kr);  % exactdiffco soft
UsnDIFF_SERIES = conj(UsnDIFF_SERIES/sqrt(2*pi*k))
UhnDIFF_SERIES = conj(UhnDIFF_SERIES/sqrt(2*pi*k))
```

Table 3: Code of the exact by integral method

```
sgm = (2*pi-alfa)/2; phi0 = ang0+sgm;  B = ang+sgm;
nu = (2*pi-2*sgm)/pi; phi = B; m = 0; U0 =  besselh(0,1,kr0);
V1 = Vd_Int(-pi-phi+phi0,r,r0,nu,k); V2 = Vd_Int(pi-phi+phi0,r,r0,nu,k);
V3 = Vd_Int(-pi-phi-phi0+2*sgm,r,r0,nu,k);
V4 = Vd_Int(pi-phi-phi0+2*sgm,r,r0,nu,k);
UsnDIFF = (V1-V2-V3+V4)/U0; % exact normalised diffracted fields
UhnDIFF = (V1-V2+V3-V4)/U0; % exact normalised diffracted fields
BWsnDIFF = UsnDIFF*sqrt(2*pi*kr)/exp(1i*kr); % diff coeff for soft BCs
BWhnDIFF = UhnDIFF*sqrt(2*pi*kr)/exp(1i*kr); % diff coeff for hard BCs
BWsnDIFF = conj(BWsnDIFF/sqrt(2*pi*k))
BWhnDIFF = conj(BWhnDIFF/sqrt(2*pi*k))
%-------------------------------------------------------------------------
% Function : Vd_Int.m (calculate Vd integral on deformed contour  )
function result = Vd_Int(beta,ro,ro0,nu,k)
   eps = 1e-12;     d = 1e-3; % step size of the integration
   Mmax = 5000; y0 = min(pi,abs(beta));  fun = 1e6;  x = y0-0.01;
    while ( abs(fun)>eps )  % controlling maximum x value
      z = x+1i*(y0-0.01);  R_it = sqrt(ro*ro+ro0*ro0+2*ro*ro0*cos(1i*z));
      fun = besselh(0,1,k*R_it)./(cosh(z/nu)-cos(beta/nu));  x = x+0.2;
    end
    xmax = x;  tan_teta = (y0-0.01)/xmax; % slope of the deformed contour
    x = 0:d:xmax;  z1 = x+1i*x*tan_teta;  % deformed contour
    R_it_1 = sqrt(ro*ro+ro0*ro0+2*ro*ro0*cos(1i*z1));
    fun1 = sin(beta/nu)*besselh(0,1,k*R_it_1)./(cosh(z1/nu)-cos(beta/nu));
    y1 = trapz(z1,fun1);    result = (y1)/(2*pi*nu);
```

Table 4: Code of the UTD method

```
phi0 = -ang0; n = (alfa)/pi; B = -ang; phi = B;
ksi_p = phi+phi0; ksi_m = phi-phi0; % ksi+ and ksi-
Npp = (pi+ksi_p)/(2*pi*n); Npm = (pi+ksi_m)/(2*pi*n);  % N+
Nmp = (-pi+ksi_p)/(2*pi*n); Nmm = (-pi+ksi_m)/(2*pi*n); % N-
m = 0; U0 =  besselh(0,1,kr0); coeff = exp(-1i*pi/4)/(2*n*sqrt(2*pi*k));
if (Npp<1) || (Npm<1) , Npp = 0; Npm = 0;
```

```
elseif (Npp>=1) || (Npm>=1), Npp = 1; Npm = 1;
end
if (Nmp<0) || (Nmm<0), Nmp = -1; Nmm = -1;
elseif (0<=Nmp<1) || (0<=Nmm<1), Nmp = 0; Nmm = 0;
elseif (Nmp>=1) || (Nmm>=1), Nmp = 1; Nmm = 1;
end
gpp = 1+cos(ksi_p-2*n*pi*Npp);  gpm = 1+cos(ksi_m-2*n*pi*Npm);
gmp = 1+cos(ksi_p-2*n*pi*Nmp); gmm = 1+cos(ksi_m-2*n*pi*Nmm);
x1 = k*r*r0*gpm/(r+r0); x2 = k*r*r0*gmm/(r+r0);
x3 = k*r*r0*gpp/(r+r0); x4 = k*r*r0*gmp/(r+r0);
F1 = Fresnel_Int(x1); F2 = Fresnel_Int(x2); F3 = Fresnel_Int(x3);
F4 = Fresnel_Int(x4);
UsDIFF_UTD = -coeff*(cot((pi+ksi_m)/(2*n))*F1+cot((pi-
ksi_m)/(2*n))*F2...
  -cot((pi+ksi_p)/(2*n))*F3-cot((pi-ksi_p)/(2*n))*F4); % coeff for soft BCs
UhDIFF_UTD = -coeff*(cot((pi+ksi_m)/(2*n))*F1+cot((pi-
ksi_m)/(2*n))*F2...
  +cot((pi+ksi_p)/(2*n))*F3+cot((pi-ksi_p)/(2*n))*F4); % coeff for hard BCs
Us_UTD=UsDIFF_UTD*sqrt(2*pi*k);
Uh_UTD=UhDIFF_UTD*sqrt(2*pi*k);
% ------------------------- Total Field for UTD -------------------------
if (ang >= 0) && (ang < pi-ang0)   % -------- Region I -------
   R1=sqrt(r*r+r0*r0-2*r*r0*cos(phi-phi0));
   R2=sqrt(r*r+r0*r0-2*r*r0*cos(phi+phi0));
   Uxs=besselh(0,1,k*R1)-besselh(0,1,k*R2);
   Uxh=besselh(0,1,k*R1)+besselh(0,1,k*R2);
   UsTOTAL_UTD = UsDIFF_UTD+Uxs/U0;
   UhTOTAL_UTD = UhDIFF_UTD+Uxh/U0;
elseif  (ang >= pi-ang0) && (ang < pi+ang0)   % -------- Region II -------
   R1=sqrt(r*r+r0*r0-2*r*r0*cos(phi-phi0)); Ux=besselh(0,1,k*R1);
   UsTOTAL_UTD = UsDIFF_UTD+Ux/U0;
   UhTOTAL_UTD = UhDIFF_UTD+Ux/U0;
elseif (ang >= pi+ang0) && (ang <= alfa)  % -------- Region III -------
   UsTOTAL_UTD = UsDIFF_UTD; UhTOTAL_UTD = UhDIFF_UTD;
end
Us_UTD = Us_UTD/sqrt(2*pi*k)
Uh_UTD = Uh_UTD/sqrt(2*pi*k)
%--------------------------------------------------------------------------
% Function : Fresnel_Int.m  (Fresnel integral)
function result = Fresnel_Int(x)
Ml = 0.3;  Mu = 5.5; coeff = 2*1i*sqrt(x)*exp(1i*x);
if (x < Ml)
result = exp(1i*(pi/4+x))*(sqrt(pi*x)-2*x*exp(1i*pi/4)-(2/3)*x*x*exp(-
1i*pi/4));
elseif (x > Mu)
   result = 1+1i/(2*x)-3/(4*x^2)-15*1i/(8*x^3)+75/(16*x^4);
else
   eps = 1e-12;  Mmax = 5000;  d = 1e-3;  y_old = 1e6; ii = 0;
   for M=sqrt(x)+1:Mmax
   ii = ii+1; t1 = sqrt(x):d:M; t2=0:d:M-sqrt(x);  t = t1-1i*t2;
   fun = exp(-1i*t.*t); y(ii) = trapz(t,fun);  error = abs(y(ii)-y_old);
   y_old = y(ii);
   if (error<eps) , result = y(ii)*coeff;  break;
   else continue
   end
   end
   result = y(ii)*coeff;
end
```

Table 5: Code of the PE diffraction method

```
n = alfa/pi; rho=r*r0/(r+r0); m=0; krho=k*rho; psi = ang-ang0;
w1 = Int_calcPE2(alfa,krho,psi)*exp(1i*(krho+pi/4))/(pi*sqrt(2));
psi = ang+ang0;
w2 = Int_calcPE2(alfa,krho,psi)*exp(1i*(krho+pi/4))/(pi*sqrt(2));
Ws=(w1-w2)*exp(-1i*krho); Wh=(w1+w2)*exp(-1i*krho);
Us_PE = Ws*sqrt(r0/(r0+r))*exp(1i*kr); % normalized PE diff field -soft
Uh_PE = Wh*sqrt(r0/(r0+r))*exp(1i*kr); % normalized PE diff field -hard
PEs_DiffCoeff = Us_PE*sqrt(2*pi*kr)/exp(1i*kr);
PEh_DiffCoeff = Uh_PE*sqrt(2*pi*kr)/exp(1i*kr);
PEs_DiffCoeff = conj(PEs_DiffCoeff)/sqrt(2*pi*k)
PEh_DiffCoeff = conj(PEh_DiffCoeff)/sqrt(2*pi*k)
%--------------------------------------------------------------------------
% Function : Int_calcPE2.m
function result = Int_calcPE2(alfa,kr,psi)
  eps = 1e-12; n = alfa/pi; y_old = 1e6; result = 0;
  for M=1:100
   s = -M:0.0001:M;  eta=sqrt(2).*s.*exp(-1i*pi/4);
   F2 = (1/n).*sin(pi/n)./(cos(pi/n)-cos((eta+psi)/n));
   fun = exp(-kr*s.*s).*F2;
   y(M) = trapz(s,fun); error = abs(y(M)-y_old); y_old = y(M);
   if (error<eps) , result = y(M);  N = M; break;
   else, continue
   end
 end
```

REFERENCES

[1] A. Sommerfeld, “Mathematische Theorie der Diffraction,” *Mathematische Annalen*, vol. 16, pp. 317-374, 1896.

[2] H. M. Macdonald, *Electric Waves*, The University Press, Cambridge, England, 1902.

[3] A. Sommerfeld, *Theorie der Beugung*, Chapter 20 in the book *“Die Differential- und Integralgleichungen der Mechanik und der Physik”*, The second (Physical) part. Editors: Ph. Frank and R. Mises, Friedr. Vieweg & Sohn, Braunschweig, Germany, 1935. American publication by Mary S. Rosenberg, New York, 1943.

[4] G. D. Malyuzhinets, “Development of Ideas about Diffraction Phenomena,” *Soviet Physics-Uspekhi*, vol. 69, no. 2, p. 5, 1959.

[5] V. A. Fock and L. A. Wainshtein, “Transverse Diffusion of Short Waves Diffracted by a Convex Cylinder, Part 1 and 2,” (in Russian) *Radiotekhnikai Elektronika*, vol. 8, no. 3, pp. 363-388, 1963. (This journal was translated into English as *Radio Engineering and Electronic Physics* by Scripta Technica.)

[6] J. J. Bowman, T. B. A. Senior, and P. L. E. Uslenghi, *Eds.*, *Electromagnetic and Acoustic Scattering by Simple Shapes*, Hemisphere Publishing Corporation, 1987.

[7] V. A. Fock, *Electromagnetic Diffraction and Propagation Problems*, Pergamon Press, London, 1965.

[8] J. B. Keller, "Geometrical Theory of Diffraction," *J. Opt. Soc. Amer.*, vol. 52, pp. 116-30, 1962.

[9] C. Hansen, *Ed.*, *Geometrical Theory of Diffraction*, IEEE Press, 1981.

[10] P. H. Pathak and R. G. Kouyoumjian, "The Dyadic Diffraction Coefficient for a Perfectly Conducting Wedge," *Technical report# 2183-4, ElectroScience Laboratory, The Ohio State University*, prepared under contract number AF19 (628)-5929 for Air Force Cambridge Research Laboratories (AFCRL), Bedford, Mass., June 1970.

[11] R. G. Kouyoumjian and P. H. Pathak, "A Uniform Geometrical Theory of Diffraction for an Edge in a Perfectly Conducting Surface," *Proc. IEEE*, vol. 62, pp. 1448-1461, 1974.

[12] P. Ya. Ufimtsev, *Fundamentals of the Physical Theory of Diffraction*, Wiley & Sons, Inc., Hoboken, New Jersey, 2007.

[13] P. Ya. Ufimtsev, *Theory of Edge Diffraction in Electromagnetics: Origination & Validation of PTD*, SciTech Publishing, Inc., 2009.

[14] F. Hacivelioglu, L. Sevgi, and P. Ya. Ufimtsev, "Electromagnetic Wave Scattering from a Wedge with Perfectly Reflecting Boundaries: Analysis of Asymptotic Techniques," *IEEE Antenn. and Propagat. Mag*., vol. 53, no. 3, pp. 232-253, 2011.

[15] G. Cakir, L. Sevgi, and P. Ya. Ufimtsev, "FDTD Modeling of Electromagnetic Wave Scattering from a Wedge with Perfectly Reflecting Boundaries: Comparisons against Analytical Models and Calibration," *IEEE Trans. on Antennas and Propagat.* (to appear) July 2012.

[16] F. Cátedra, L. Lozano, I. González, E. García, and M. Algar, "Efficient Techniques for Accelerating the Ray-Tracing for Computing the Multiple Bounce Scattering of Complex Bodies Modeled by Flat Facets," *Applied Computational Electromagnetics Society (ACES) Journal*, vol. 25, no. 5, pp. 395–409, May 2010.

[17] F. Weinmann, "UTD Shooting-and-Bouncing Extension to a PO/PTD Ray Tracing Algorithm," *Applied Computational Electromagnetics Society (ACES) Journal*, vol. 24, no. 3, pp. 281–293, June 2009.

[18] R. H. Hardin, and F. D. Tappert, "Applications of the Split-Step Fourier Method to the Numerical Solution of Nonlinear and Variable Coefficient Wave Equations," *SIAM Rev.*, vol. 15, p. 423, 1973.

[19] J. R. Kuttler and G. D. Dockery, "Theoretical Description of the Parabolic Approximation / Fourier Split-Step Method of Representing Electromagnetic Propagation in the Troposphere," *Radio Sci*., vol. 26, pp. 381-393, 1991.

[20] M. F. Levy, *Parabolic Equation Methods for Electromagnetic Wave Propagation*, IEEE Electromagnetic Wave Series, London, 2000.

[21] L. Sevgi, *Complex Electromagnetic Problems and Numerical Simulation Approaches*, IEEE Press/John Wiley, New York, 2003.

[22] G. Apaydın and L. Sevgi, "Validation, Verification and Calibration in Applied Computational Electromagnetics", *Applied Computational Electromagnetics Society (ACES) Journal*, vol. 25, no. 12, pp. 1026-1035, Dec. 2010.

[23] O. Ozgun, "Recursive Two-Way Parabolic Equation Approach for Modeling Terrain Effects in Tropospheric Propagation," *IEEE T Antenn. Propag*., vol. 57, no. 9, pp. 2706-2714, Sept. 2009.

[24] O. Ozgun, G. Apaydin, M. Kuzuoglu, and L. Sevgi, "Two-Way Fourier Split Step Algorithm over Variable Terrain with Narrow and Wide Angle Propagators," *IEEE Int. Symp. on Antenn. and Propag*., ON, Canada, 2010.

[25] O. Ozgun, G. Apaydin, M. Kuzuoglu, and L. Sevgi, "PETOOL: MATLAB-Based One-Way and Two-Way Split-Step Parabolic Equation Tool for Radiowave Propagation over Variable Terrain," *Computer Physics Communications*, vol. 182, no. 12, pp. 2638–2654, Dec. 2011.
Associated program is available at: http://cpc.cs.qub.ac.uk/summaries/AEJS_v1_0.html

[26] F. Hacıvelioğlu, L. Sevgi, P. Ya. Ufimtsev, "Electromagnetic Wave Scattering from a Wedge with Perfectly Reflecting Boundaries: Analysis of Asymptotic Techniques," *IEEE Antennas and Propagation Magazine*, vol. 53, no. 3, pp. 232-253, June 2011.

Özlem Özgün received the Ph.D. degree in Electrical Engineering from Middle East Technical University (METU), Ankara, Turkey, in 2007. She was with the same university between 2008-2012. She is now an associate professor in TED University, Ankara, Turkey. Her main research interests are computational electromagnetics, finite element method, domain decomposition, electromagnetic propagation and scattering, metamaterials, and stochastic electromagnetic problems.

Levent Sevgi has been with Dogus University since 2002. He has involved in complex electromagnetic problems for more than two decades. He is also interested in novel approaches in engineering education, teaching electromagnetics via virtual tools and popular science.

He is a member of Turkish Chamber of Electrical Engineers (EMO), a Fellow member of the IEEE, an assoc. Editor, of the IEEE Antennas and Propagation Magazine, "Testing ourselves" Column and member of the IEEE Antennas and Propagation Society Education Committee.